www.sciencemag.org/cgi/content/full/336/6089/1723/DC1

Supplementary Materials for

CTD Tyrosine Phosphorylation Impairs Termination Factor Recruitment to RNA Polymerase II

Andreas Mayer, Martin Heidemann, Michael Lidschreiber, Amelie Schreieck, Mai Sun, Corinna Hintermair, Elisabeth Kremmer, Dirk Eick,* Patrick Cramer*

*To whom correspondence should be addressed. E-mail: eick@helmholtz-muenchen.de (D.E.); cramer@genzentrum.LMU.de (P.C.)

Published 29 June 2012, *Science* **336**, 1723 (2012)
DOI: 10.1126/science.1219651

This PDF file includes:

Materials and Methods

Generation of the 3D12 monoclonal antibody

The antibody was generated as previously described (*7*). For immunization we used the CTD-specific phosphopeptide YSPTSPKme2Y(P)SPTSPSC (PSL GmbH, Heidelberg, Germany, (P) refers to the phosphate at the preceding Y residue) coupled to ovalbumin. The rat monoclonal antibody 1C7 (IgG2a) recognizes unphosphorylated and different phosphorylated forms of the CTD (fig. S1).

Characterization of the 3D12 antibody

For further characterization of specificity, antibodies were analyzed in ELISA experiments using CTD-like peptides with different modification patterns (Peptide Specialty Laboratories GmbH, Heidelberg, Germany) coupled to 96-well maleimide plates (Thermo Fisher Scientific Inc., Rockford, IL USA) as antigen (fig. S1). Peptides were incubated with the monoclonal antibodies and biotinylated, subclass-specific antibodies respectively. After incubation with horseradish peroxidase (HRP)-coupled avidin, H_2O_2 and TMB (3,3',5,5'-tetramentylbenzidine) was added. Absorbance of each well was measured at 650 nm after color change and quantitated with an ELISA reader.

Immunoprecipitation (IP) for antibody validation

HeLa cells were washed twice with cold PBS and lysed in 100 µl lysis buffer per $3x10^6$ cells (50 mM Tris-HCl, pH 8.0, 150 mM NaCl, 1% NP-40 (Roche), 1x PhosSTOP (Roche), 1x protease inhibitor cocktail (Roche) for 30 min on ice. All samples were sonicated on ice using a BRANSON Sonifier 250 (15 sec on, 15 sec off, 50% duty) and centrifuged at 16,400 rpm (FA-45-24-11 rotor) for 20 min at 4°C. The supernatant was incubated with antibody-coupled protein G-Sepharose beads (2.5 µg of antibodies for 4 h at 4 °C, followed by 3 washes with 1 ml IP buffer) rotating overnight. Beads were washed 5 times with 1ml lysis buffer before continuative experiments. For IPs from yeast, logarithmically grown cells (OD_{600} = 0.8) were pelleted, washed and lysed in 1 ml lysis buffer (50 mM HEPES-KOH, pH 7.5, 150 mM NaCl, 1 mM EDTA, 1% Triton X-100, 0.1% sodium deoxycholate) with phosphatase/protease inhibitors per 50 ml cells. After centrifugation (13,000 rpm, FA-45-24-11 rotor for 30 min at 4°C) the supernatant was added to the antibody-precoupled beads respectively. After overnight incubation, the beads were washed 5 times with lysis buffer (+ inhibitors) and proteins were boiled off Sepharose beads in Laemmli buffer (2% SDS, 10% glycerol, 60 mM TrisHCl, pH 6.8, 10 mM EDTA, 1 mM PMSF, 100 mM DTT, 0.01% bromophenol blue) for SDS-PAGE.

In vitro c-Abl kinase assay

Immuno-purified Pol II from whole cell extracts with an antibody recognizing unphosphorylated CTD (1C7) was used as substrate for kinase assays. 10 µl of the substrate coupled Sepharose G beads were incubated with 40 µl tyrosine kinase buffer (5x kinase buffer A: 300 mM HEPES, pH 7.5, 15 mM $MgCl_2$, 15 mM $MnCl_2$, 6 mM DTT, 15 mM Na_3VO_4, 12.5 µM PEG 20,000) or serine kinase buffer (5x kinase buffer B: 250 mM HEPES, pH 7.9, 50 mM $MgCl_2$, 500 mM KCl, 5 mM DTT, 1 mM EGTA, 500 µM EDTA), 200 µM ATP, 1 µg BSA and 200 ng of the recombinant kinase (ProQinase GmbH, Freiburg, Germany) at 30°C for 30 minutes. 10 µl of 6x Laemmli buffer was

added and samples were boiled for 7 minutes at 95°C followed by SDS-PAGE and western analysis.

Chromatin immunoprecipitation (ChIP) upon kinase inhibition

ChIP experiments were performed as described (*31*), but with the following modifications. First, analog-sensitive (as) kinase yeast strains (*32*) were grown in 100 ml YPD medium at 30°C to OD_{600} ~ 0.6. Then the culture was split in two 50 ml cultures. One culture was treated with the respective kinase inhibitor (dissolved in DMSO) and the other one with DMSO only, serving as a solvent control. For kinase inhibition the following inhibitors were applied: 20 µM of 3-MB-PP1for Bur1 inhibition, 10 µM 1-NM-PP1 for Ctk1 and Srb10 inhibition, and 5 µM 1-NA-PP1 for Kin28 inhibition. After addition of the kinase inhibitor or the solvent control, cultures were further grown to an OD_{600} of ~0.8 (45 min) and crosslinked as described recently. Second, cell lysis and chromatin preparation was conducted in the presence of phosphatase inhibitors (1 mM NaN_3, 1 mM NaF, 0.4 mM Na_3VO_4). Third, for chromatin immunoprecipitation monoclonal antibodies with strong specificity and affinity against different phosphorylation states of the Pol II CTD, Ser5-P (3E8), Ser2-P (3E10) and Tyr1-P (3D12) as well as an antibody against the Pol II subunit Rpb3 (1Y26, NeoClone Biotechnology) were applied. 700 µl chromatin were immunoprecipitated with 25 µl 3E8, 20 µl 3E10, 100 µl 3D12 and 5 µl 1Y26 for 18 h at 4°C. Next, 25 µl of Protein G and Protein A Sepharose 4 Fast Flow (GE Healthcare) were added and incubated for another 1.5 h at 4°C. Immunoprecipitated chromatin was further processed and analyzed by quantitative realtime PCR essentially as described recently (*14*).

Genome-wide signal profiling

Chromatin immunoprecipitation was performed as described (*14*). Briefly, 600 ml of yeast were grown in YPD medium to mid-log phase and treated with 1% (v/v) formaldehyde for 20 min at 20°C. Cells were lysed by bead beating with silica-zirconia beads for 60 min. Chromatin was resolubilized and sheared by sonication (Bioruptor UCD-200, Diagenode) for 35 min at 4°C. For TAP-tagged proteins, immunoprecipitation (IP) was performed with IgG Sepharose beads (GE Healthcare) for 3 h at 4°C. For the Tyr1 and Thr4 Pol II phospho-isoforms, IP was performed with 100 µl 3D12 and 100 µl 6D7 monoclonal antibodies, respectively. IP was conducted in the presence of the respective monoclonal antibody over-night at 4°C and then incubated with Protein A and G Sepharose beads (GE Healthcare) for 1.5 h at 4°C. After several washing steps and the elution from Sepharose beads, crosslinks were reversed by heating with Proteinase K over-night. DNA was purified and RNA was digested by RNase A. DNA was amplified with the Whole Genome Amplification 2 Kit (Sigma) according to the manufacturer's instructions. 5.5 µg of DNA was hybridized onto a custom-made Affymetrix tiling array that covers the yeast genome at 4 nts resolution (*33*). At least two biological replicates were analyzed. ChIP-chip of the Tyr1 and Thr4 Pol II phospho-isoform was carried out in the presence of phosphatase inhibitors (1 mM NaN_3, 1 mM NaF, 0.4 mM Na_3VO_4).

ChIP-chip data normalization

Normalization of ChIP-chip data was performed as described recently (*14*). First, we performed quantile normalization between replicate measurements (not between non-

replicate measurements). Second, for each condition (including the reference measurements) we averaged the signal for each probe by calculating the geometric average over the replicate intensities. Third, IP data from all factors and Pol II phospho-isoforms were normalized by dividing through genomic input intensities. Data was smoothed using running median smoothing with a window half size of 75 bp.

Gene-averaged occupancy profiles

Gene-averaged profiles were generated as described recently (*14*). Briefly, the normalized ChIP-chip signal ($\log_2$ IP/Input) at each nucleotide was calculated as the median signal of all probes overlapping this position. To average profiles over genes, yeast genes were filtered. Of 4,366 yeast genes with annotated TSS and pA sites (*34*), we examined the 50% most highly expressed genes (*15*) that were at least 200 nts away from neighboring genes (ALL gene set, 1140 genes). Three ORF length classes were defined, Short (S, 512 to 937 bp), Medium (M, 938 to 1537 bp), and Long (L, 1538 to 2895 bp), comprising 266, 339, and 299 filtered genes, respectively. Profiles within these groups were scaled to median gene length and the gene-averaged profiles were calculated by taking the median over genes at each genomic position.

Pairwise profile correlations

Correlation analysis was done using 4,366 genes with TSS and pA annotations (*34*). Pairwise Pearson correlations over factor occupancy profiles were calculated between concatenated gene profiles ranging each from TSS-250 bp to pA+250 bp.

Singular value decomposition (SVD)

SVD analysis was performed as described recently (*14*). Briefly, for each of the Pol II phospho-isoforms f and for each of the 4,366 genes g for which we had TSS and pA annotations (*34*), we calculated 90%-quantiles of ChIP-chip signals within a region [TSS-250bp, pA+250bp] as a robust proxy for peak occupancies. This resulted in a 3×4,366 matrix. From each matrix element, we subtracted the average over its row. The resulting matrix X_{fg} was subjected to SVD, yielding singular values $\sigma_1 \geq \sigma_2 \geq \sigma_3 \geq 0$ and unit-length, orthogonal, singular vectors u_1, u_2, u_3, v_1, v_2, v_3, such that $X_{fg} = \Sigma_{i=1,..,3}\ \sigma_i \times u_{if} \times v_{ig}$. The k'th term in this sum, $\sigma_k \times u_{kf} \times v_{kg}$, can explain a fraction $\sigma_k^2/\Sigma_i\ \sigma_i^2$ of the data variance.

Protein sample preparations

The DNA sequence coding for the *S. cerevisiae* Nrd1-CID (residues 6-151 (*16*)), Pcf11-CID (residues 1-140 (*22*)) and Rtt103-CID (residues 1-131 (*23*)) was cloned into a pET28b plasmid, resulting in an N-terminal hexahistidine tagged protein version. Proteins were expressed in *E. coli* BL21 (DE3) RIL cells (Stratagene) in 1 L LB medium for 16 h at 18°C. Cells were harvested, washed with PBS buffer, and lysed by sonication in the presence of buffer A (50 mM Tris-HCl, pH 8.0, 300 mM NaCl, 10 mM β-Mercaptoethanol). The lysate was cleared by centrifugation and the supernatant was loaded on a Ni-NTA column (Qiagen). The Pcf11-CID was further purified as previously described (*22*). For further purification of the Nrd1-CID the eluate of Ni-NTA column was applied to cation exchange chromatography (Mono S, GE Healthcare). The column was equilibrated with buffer B (50 mM MES, pH 6.5, 50 mM NaCl, 1 mM DTT), and Nrd1-CID was eluted with a linear gradient of 20 column volumes from 50 mM to 1 M

NaCl. After concentration, the sample was applied to a Superose 12 size exclusion column (GE Healthcare) equilibrated with buffer C (50 mM HEPES, pH 7.5, 100 mM NaCl, 1 mM DTT). For further purification of the Rtt103-CID, the eluate of the Ni-NTA column was concentrated and the sample was applied to a Superdex 75 size exclusion column (GE Healthcare) equilibrated with buffer C. The Spt6 tandem SH2 domain (residue 1250-1444) from *Candida glabrata* was recombinantly expressed in *E. coli* cells and purified essentially as described recently (*24*). Pooled peak fractions of Nrd1-, Pcf11-, Rtt103-CID and of the Spt6 tandem SH2 domain were concentrated to 5-10 mg/ml and stored at -80°C.

Pol II CTD phosphopeptide interaction assay

Fluorescence anisotropy measurements were carried out with a HORIBA Jobin-Yvon Fluoromax 3 spectrofluorometer as described in the Methods Summary. The CTD peptides used are listed in Table S1. For Pcf11-CID measurements were performed in the presence of 10 mM NaCl (Fig. 3A) and 150 mM NaCl (fig. S7). For Rtt103-CID (Fig. 3B) and Nrd1-CID (Fig. 3C) fluorescence anisotropy was determined in the presence of 150 mM NaCl, and for the Spt6 tandem SH2 domain (Fig. 3D) in the presence of 10 mM NaCl. A fixed amount of the respective N-terminally fluorescein labeled CTD peptide (500 nM) was titrated with the protein of interest. After equilibration was reached (2 min) the fluorescence anisotropy values (technical triplicates) were measured at each concentration and used, if possible, to generate a binding isotherm. The binding isotherm was generated by non-linear regression analyses (Hill curve fit) with the software package OriginPro 8G (OriginLab Corporation, Northampton). Based on this binding curve, the dissociation constant (K_D) was calculated as the protein concentration where ΔAnisotropy was half maximal (μM range). This was also carried out in OriginPro 8G.

Phospho-peptide		Phospho-site	αTyr1-P 3D12	1C7	αThr4-P 6D7
CTD-1	YSPTSPSYSPTSPSC	-	-	+++	-
CTD-2	YSP^{P}TSPSYSPTSPSC	T_4	-	++	+++
CTD-3	YSP^{PP}TSPSYSPTSPSC	T_4,S_5	-	-	-
CTD-4	YSPT^{P}SPSYSPTSPSC	S_5	-	-	-
CTD-5	YSPTSPS^{P}YSPTSPSC	S_7	-	+++	-
CTD-6	YSPTSPSY^{P}SPTSPSC	Y_1	+++	+++	-
CTD-7	YSPTSPSYS^{P}PTSPSC	S_2	-	+++	-
CTD-8	YSPT^{P}SPSYS^{P}PTSPSC	S_5,S_2	-	-	-
CTD-9	SPSYS^{P}PT^{P}SPSYSPTC	S_2,S_5	-	-	-
CTD-10	YSPTSPSY^{PP}SPTSPSC	Y_1,S_2	+++	+++	-
CTD-11	YSPT^{P}SP^{P}SYSPTSPSC	S_5,S_7	-	-	-
CTD-12	YSPTSPS^{P}YS^{P}PTSPSC	S_7,S_2	-	+++	-
CTD-13	YSPTSPSY^{P}SPT^{P}SPSC	Y_1,T_4	-	+++	+++
CTD-14	YSPTSPSY^{P}SPTS^{P}PSC	Y_1,S_5	-	+++	-
CTD-15	YSP^{P}TSPSY^{P}SPTSPSC	T_4,Y_1	-	-	+++
CTD-16	YSPT^{P}SPSY^{P}SPTSPSC	S_5,Y_1	-	-	-
CTD-17	YSPTSPS^{PP}YSPTSPSC	S_7,Y_1	-	+++	-
CTD-18	YSPTSPSYS^{P}PT^{P}SPSC	S_2,T_4	-	+++	+
CTD-19	YSP^{P}TSPS^{P}YSPTSPSC	T_4,S_7	-	-	+++

Fig. S1

Specificity of α-Tyr1-P antibody 3D12, 1C7 and α-Thr4-P antibody 6D7. Panel of CTD phosphopeptides used for antibody characterization. The phosphosites and the reactivity in ELISA assays are indicated (High "+++", medium "++", low "+" and no "-" reactivity).

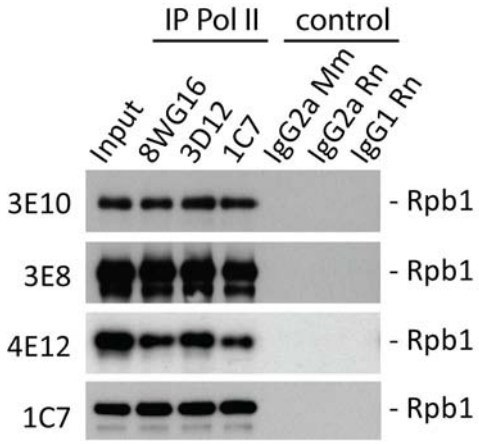

Fig. S2

Co-occurrence of Pol II CTD phosphorylation marks. Western blot analysis of whole cell extract from proliferating yeast (Input). Pol II was immunoprecipitated with antibodies 8WG16, 3D12 and 1C7 (IP Pol II) and probed with 3E10 (αSer2-P), 3E8 (αSer5-P), 4E12 (αSer7-P) and 1C7. Isotype controls are shown. Please also refer to Fig. 1B.

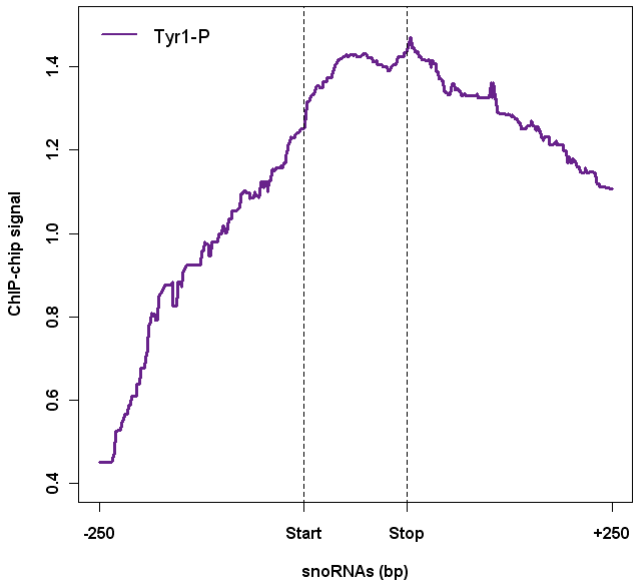

Fig. S3

Tyr1 phosphorylation ChIP-chip signal averaged over snoRNA genes.

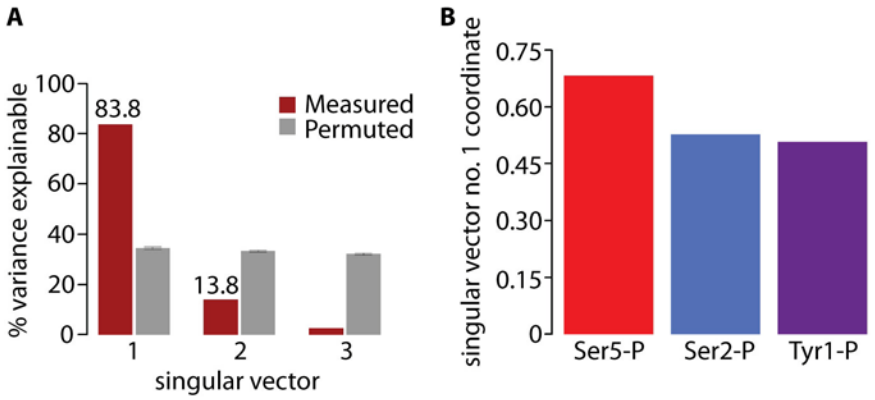

Fig. S4

CTD Tyr1 phosphorylation, like Ser2 and Ser5 phosphorylation, is a general type of CTD modification. **(A)** Singular value decomposition (SVD) analysis of Ser2-P, Ser5-P, and Tyr1-P genome-wide ChIP signals. The contributions of the first three singular vectors to the variance (red) are shown in comparison to a control with randomly permuted matrix elements (gray). SVD reveals that 83.8% of the variance is explained by covariation. **(B)** Coefficients of first left singular vector for the SVD of the occupancy matrix for the three Pol II phospho-isoforms. The first eigenvector with its similar-sized coefficients describes the co-variation of all three Pol II phospho-isoforms.

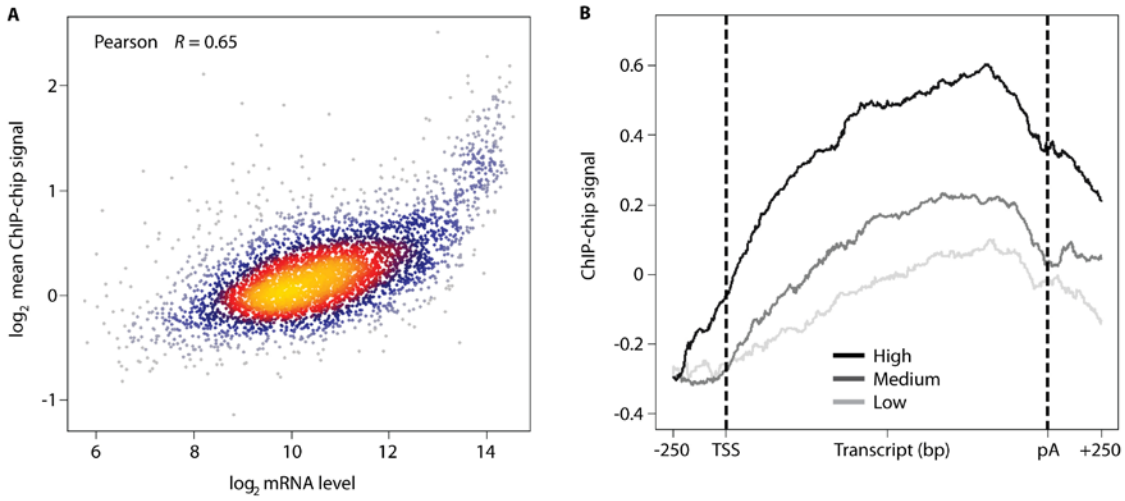

Fig. S5

CTD Tyr1 phosphorylation levels correlate with mRNA expression in proliferating yeast. **(A)** Gene-wise correlation analysis between the logarithm of the average Tyr1-P ChIP-chip signal and the logarithm of mRNA levels. **(B)** Gene-averaged profiles for genes in three different mRNA expression level classes. The genes were partitioned into three groups: low (25-50% quantile), medium (50-75% quantile) and high (>75% quantile) expression according to published data (*15*). From this set of genes, those with ORF lengths between 938 and 1538 were selected.

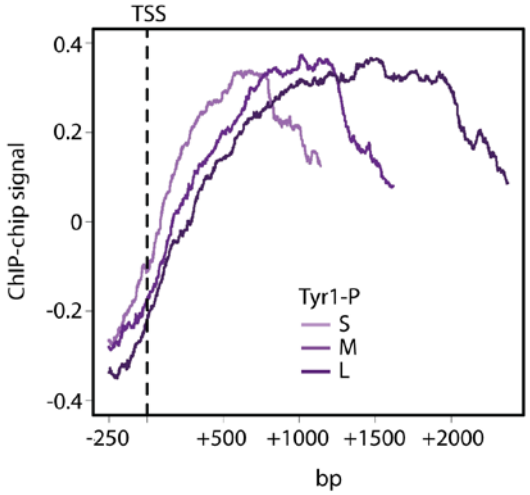

Fig. S6

Additional evidence that CTD Tyr1 phosphorylation occurs in the transcription cycle. Gene-averaged Tyr1 phosphorylation ChIP-chip signals of three gene length classes ("small/S": 725 ± 213 nt, 266 genes; "medium/M": 1,238 ± 300 nt, 339 genes; "long/L": 2,217 ± 679 nt, 299 genes;) aligned at their TSS. The point where Tyr1 phosphorylation levels start to increase depends on the distance to the TSS.

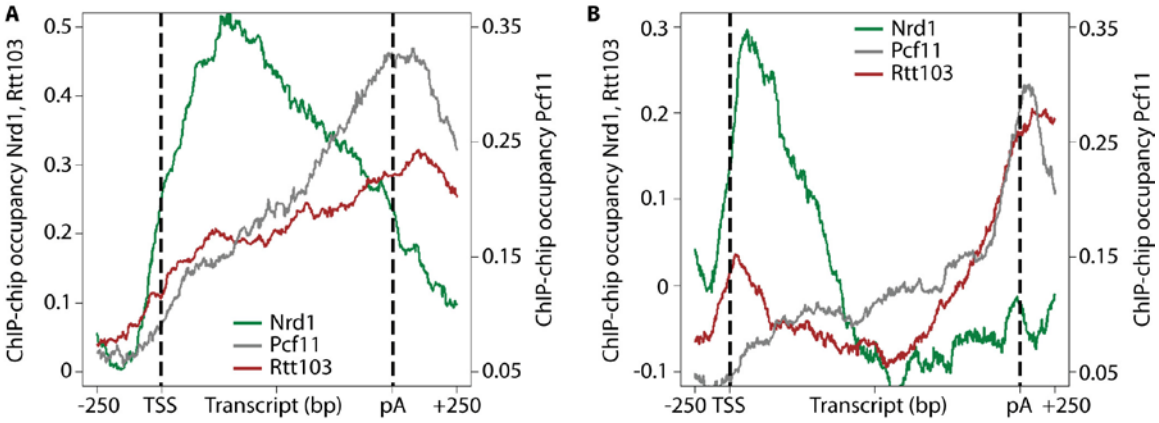

Fig. S7

Genome-wide occupancy of CTD-binding termination factors for different gene length classes. **(A)** Gene-averaged profiles for Pol II termination factors Nrd1, Pcf11 (*14*) and Rtt103 at "small" gene-length class genes (725 ± 213 nt, 266 genes). ChIP-chip occupancy of Nrd1 and Rtt103 is on the left y-axis, the occupancy of Pcf11 is on the right y-axis. **(B)** Gene-averaged profiles as in (A) but for "long" genes (2,217 ± 679 nt, 299 genes). The color code is as in Fig. 2.

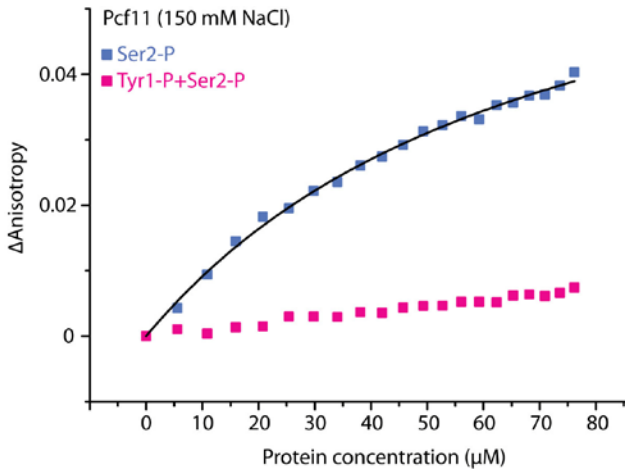

Fig. S8

Pcf11-CID binds to Ser2-phosphorylated CTD peptide, but not to a CTD peptide that is doubly phosphorylated at Ser2 and Tyr1, under high-salt conditions. The fluorescence anisotropy measurement was carried out in the presence of 150 mM NaCl (instead of 10 mM). The Pcf11-CID still binds to the Ser2-P CTD peptide at high salt conditions, but with a slightly reduced affinity (K_D = 70±18 μM instead of 54 ± 6 μM). However, the slight increase in the ΔAnisotropy that was detected for the Tyr1-P+Ser2-P CTD peptide at 10 mM NaCl (Fig. 3A), disappeared at higher salt conditions. This indicates that Pcf11-CID associates specifically with the Ser2-phosphorylated form of the Pol II CTD.

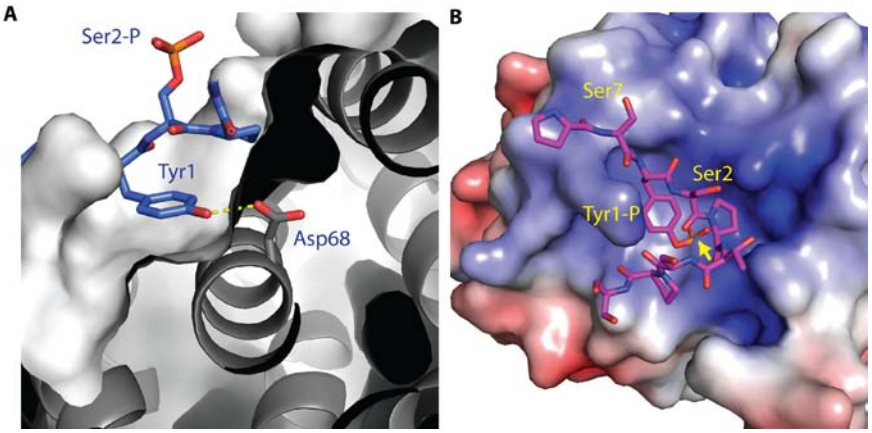

Fig. S9

Structural data explain how Tyr1 phosphorylation blocks CID-CTD interaction. **(A)** Cutaway view of the Pcf11-CID (gray) complex with a Ser2-phosphorylated CTD peptide (blue) (*22*). The Tyr1 residue of the CTD peptide forms a hydrogen bond (dashed yellow line) with the carboxyl group of the highly conserved Asp68 residue side chain in α-helix 4 of Pcf11-CID. **(B)** Structural model of Pcf11-CID (*22*) bound to Tyr1-phosphorylated CTD peptide. The modeled phosphate group on Tyr1 results in a steric

clash (yellow arrow) with Pcf11-CID. The phosphogroup on Ser2 was removed for clarity. Structural modeling and generation of Figures was done with PyMOL version 1.4.1. The surface charges were calculated with APBS. Positively and negatively charged surface areas are colored blue and red, respectively.

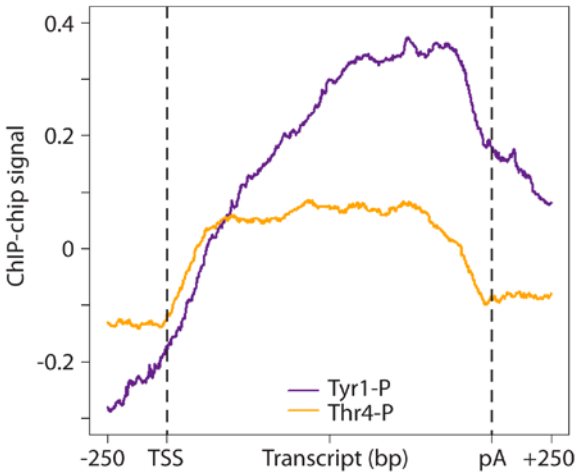

Fig. S10

ChIP-chip profiling of Tyr1- and Thr4-phosphorylated Pol II. Shown are gene-averaged profiles for the 'medium' gene-length class (1,238 ± 300 nt, 339 genes).

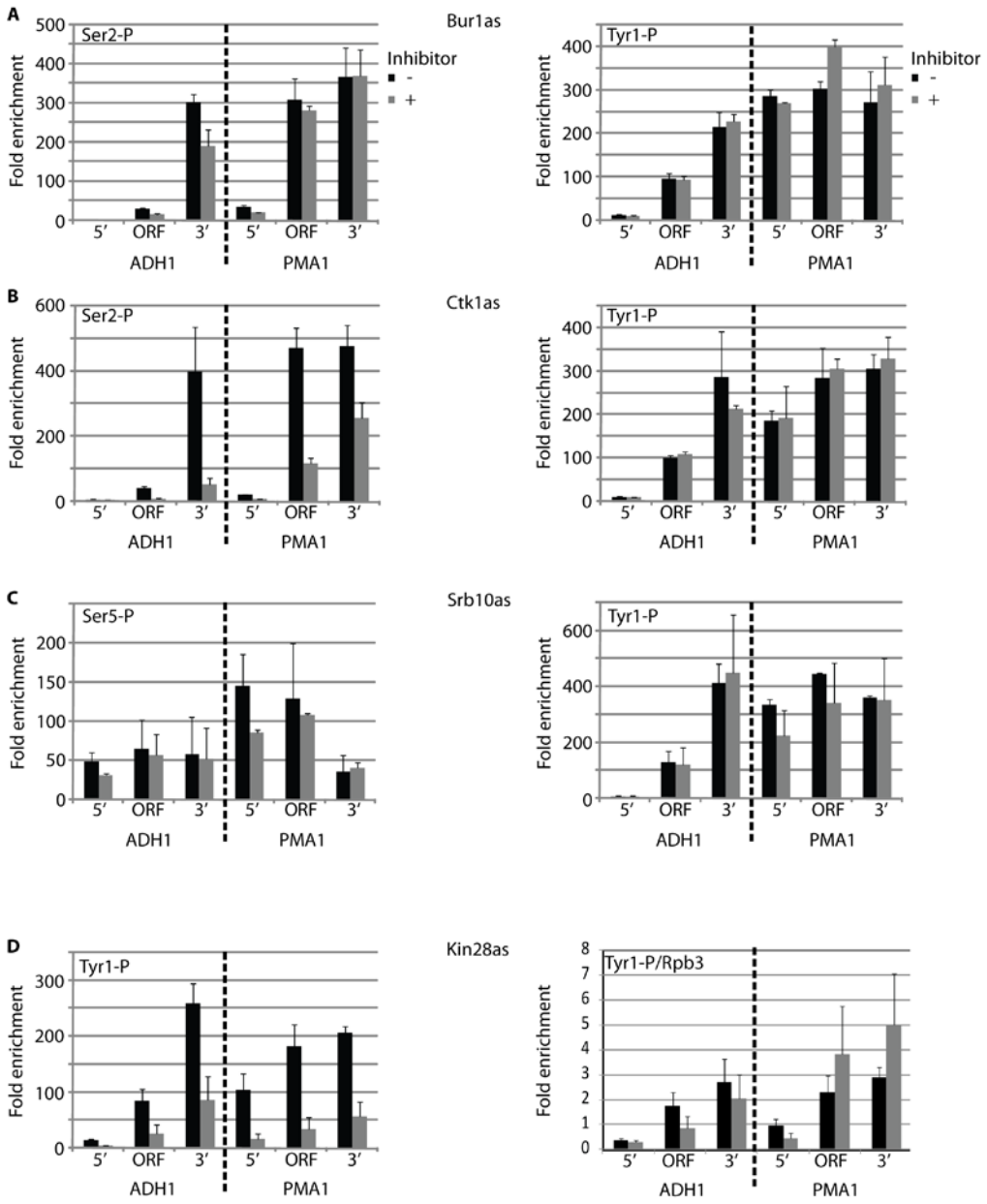

Fig. S11

CTD Tyr1 phosphorylation levels are not changed upon inhibition of the canonical Pol II CTD kinases. Kinase inhibition and ChIP experiments were performed with analog-sensitive (as) yeast strains (*32*) (Table S2) as described in the Supplementary Methods. **(A)** Bur1as strain was inhibited with the small molecule inhibitor 3-MB-PP1. Bur1 inhibition slightly reduces Ser2-P phosphorylation levels at the coding region ("ORF") of *ADH1* (p-value: 0.02; T-test) and the 5' region of *PMA1* (p-value: 0.05; left panel). These results agree with earlier observations (*35*). However, Bur1 inhibition did not change Tyr1-P levels (right panel). **(B)** Ctk1as strain was inhibited with 1-NM-PP1. Ctk1 inhibition significantly reduces Ser2-P occupancy levels as expected (p-values ≤ 0.05; left panel), serving as a positive control, whereas Tyr1-P levels were not altered (right

panel). **(C)** Srb10as strain was inhibited with 1-NM-PP1. Srb10 inhibition neither changes Ser5-P occupancy levels nor the corresponding levels of Tyr1-P. **(D)** Kin28as was inhibited with 1-NA-PP1. Kin28 inhibition leads to a reduction of Tyr1-P levels over the whole length of the transcribed region (left panel). However, this was apparently due to an overall reduction of Pol II occupancy upon Kin28 inhibition as the ratios between Tyr1-P and Pol II subunit Rpb3 ChIP occupancies do not change within the range of the standard deviation (right panel). ChIP occupancies of Pol II and of its different phosphorylated forms before and after kinase inhibition are indicated as black and gray bars, respectively. Results are shown for three different regions of the ADH1 and PMA1 gene. Fold enrichment values refer to a heterochromatic region on chromosome V that is not transcribed by Pol II. Standard deviations refer to at least two biological replicate measurements

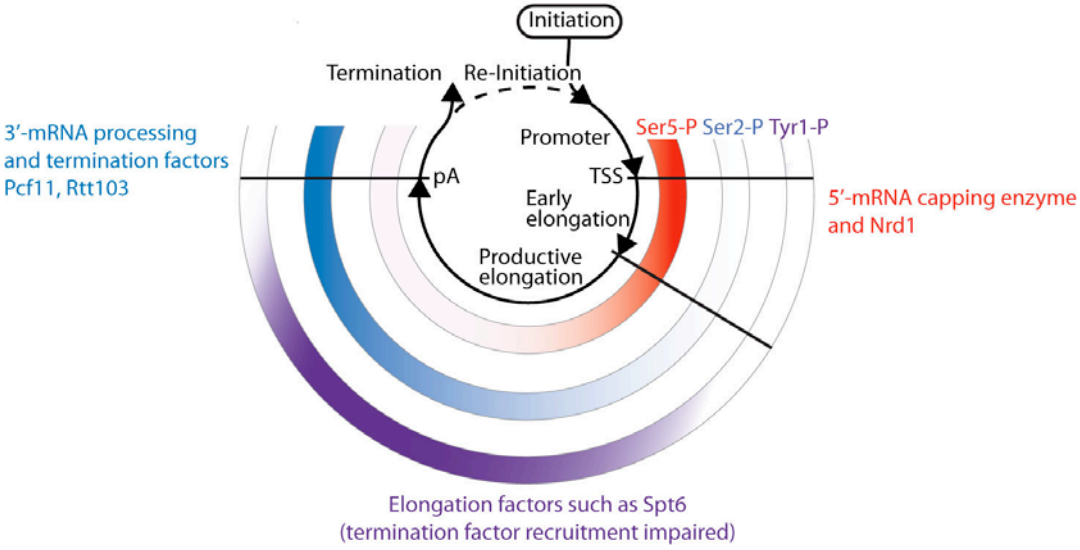

Fig. S12

Extended CTD code for transcription cycle coordination. During the cycle, levels of CTD phosphorylation at Tyr1, Ser2, and Ser5 residues change differently, as illustrated by gradients of red (Ser5-P), blue (Ser2-P) and violet (Tyr1-P) in three semicircles. Color code as in Fig. 2.

Table S1.

Synthetic CTD peptides used for *in vitro* binding studies. All CTD peptides were N-terminally labeled with fluorescein aminocaproic acid. Phosphorylated residues are highlighted on black ground.

Name	Amino acid sequence	Company
No-P	S_7 Y_1 S_2 P_3 T_4 S_5 P_6 S_7 Y_1 S_2 P_3 T_4 S_5 P_6 S_7	PANATecs
1,1	P_6 S_7 Y_1 S_2 P_3 T_4 S_5 P_6 S_7 Y_1 S_2 P_3 T_4 S_5 P_6 S_7	PSL
2,2	S_7 Y_1 S_2 P_3 T_4 S_5 P_6 S_7 Y_1 S_2 P_3 T_4 S_5 P_6 S_7	PANATecs
5,5	P_6 S_7 Y_1 S_2 P_3 T_4 S_5 P_6 S_7 Y_1 S_2 P_3 T_4 S_5 P_6 S_7	PSL
1,2,1,2	P_6 S_7 Y_1 S_2 P_3 T_4 S_5 P_6 S_7 Y_1 S_2 P_3 T_4 S_5 P_6 S_7	PSL
1,5,1,5	P_6 S_7 Y_1 S_2 P_3 T_4 S_5 P_6 S_7 Y_1 S_2 P_3 T_4 S_5 P_6 S_7	PSL

Table S2.

Analog-sensitive yeast strains (*32*) used in this study. All analog-sensitive yeast strains were kindly provided by the Hahn laboratory (Fred Hutchinson Cancer Research Center, Seattle).

Name	Genotype
Bur1as	Mat a, *his3Δ1, leu2Δ0 met15Δ0, ura3Δ0*, Bur1 L149G – Flag3::KanMX
Ctk1as	Mat α, *Δade2::hisG, his3Δ200, leu2Δ0, lys2Δ0, met15Δ0, trp1Δ63, ura3Δ0*, Ctk1 F260G – Flag3::KanMX
Kin28as	Mat α, *Δade2::hisG, his3Δ200, leu2Δ0, lys2Δ0, met15Δ0, trp1Δ63, ura3Δ0*, Kin28 L83G
Srb10as	Mat α, *Δade2::hisG, his3Δ200, leu2Δ0, lys2Δ0, met15Δ0, trp1Δ63, ura3Δ0*, srb10Δ::KanMX, pSH599 (ars cen TRP1 srb10as-1 (Y236G))

References and Notes

1. R. D. Chapman, M. Heidemann, C. Hintermair, D. Eick, Molecular evolution of the RNA polymerase II CTD. *Trends Genet.* **24**, 289 (2008). doi:10.1016/j.tig.2008.03.010 Medline

2. S. Buratowski, Progression through the RNA polymerase II CTD cycle. *Mol. Cell* **36**, 541 (2009). doi:10.1016/j.molcel.2009.10.019 Medline

3. J. L. Corden, Transcription. Seven ups the code. *Science* **318**, 1735 (2007). doi:10.1126/science.1152624 Medline

4. P. Komarnitsky, E.-J. Cho, S. Buratowski, Different phosphorylated forms of RNA polymerase II and associated mRNA processing factors during transcription. *Genes Dev.* **14**, 2452 (2000). doi:10.1101/gad.824700 Medline

5. S. C. Schroeder, B. Schwer, S. Shuman, D. Bentley, Dynamic association of capping enzymes with transcribing RNA polymerase II. *Genes Dev.* **14**, 2435 (2000). doi:10.1101/gad.836300 Medline

6. S. H. Ahn, M. Kim, S. Buratowski, Phosphorylation of serine 2 within the RNA polymerase II C-terminal domain couples transcription and 3′ end processing. *Mol. Cell* **13**, 67 (2004). doi:10.1016/S1097-2765(03)00492-1 Medline

7. R. D. Chapman *et al*., Transcribing RNA polymerase II is phosphorylated at CTD residue serine-7. *Science* **318**, 1780 (2007). doi:10.1126/science.1145977 Medline

8. M. Kim, H. Suh, E.-J. Cho, S. Buratowski, Phosphorylation of the yeast Rpb1 C-terminal domain at serines 2, 5, and 7. *J. Biol. Chem.* **284**, 26421 (2009). doi:10.1074/jbc.M109.028993 Medline

9. S. Egloff *et al*., Serine-7 of the RNA polymerase II CTD is specifically required for snRNA gene expression. *Science* **318**, 1777 (2007). doi:10.1126/science.1145989 Medline

10. J.-P. Hsin, A. Sheth, J. L. Manley, RNAP II CTD phosphorylated on threonine-4 is required for histone mRNA 3′ end processing. *Science* **334**, 683 (2011). doi:10.1126/science.1206034 Medline

11. R. Baskaran, M. E. Dahmus, J. Y. Wang, Tyrosine phosphorylation of mammalian RNA polymerase II carboxyl-terminal domain. *Proc. Natl. Acad. Sci. U.S.A.* **90**, 11167 (1993). doi:10.1073/pnas.90.23.11167 Medline

12. J. W. Stiller, M. S. Cook, Functional unit of the RNA polymerase II C-terminal domain lies within heptapeptide pairs. *Eukaryot. Cell* **3**, 735 (2004). doi:10.1128/EC.3.3.735-740.2004 Medline

13. R. Baskaran, S. R. Escobar, J. Y. J. Wang, Nuclear c-Abl is a COOH-terminal repeated domain (CTD)-tyrosine (CTD)-tyrosine kinase-specific for the mammalian RNA polymerase II: Possible role in transcription elongation. *Cell Growth Differ.* **10**, 387 (1999). Medline

14. A. Mayer *et al*., Uniform transitions of the general RNA polymerase II transcription complex. *Nat. Struct. Mol. Biol.* **17**, 1272 (2010). doi:10.1038/nsmb.1903 Medline

15. S. Dengl, A. Mayer, M. Sun, P. Cramer, Structure and in vivo requirement of the yeast Spt6 SH2 domain. *J. Mol. Biol.* **389**, 211 (2009). doi:10.1016/j.jmb.2009.04.016 Medline

16. L. Vasiljeva, M. Kim, H. Mutschler, S. Buratowski, A. Meinhart, The Nrd1-Nab3-Sen1 termination complex interacts with the Ser5-phosphorylated RNA polymerase II C-terminal domain. *Nat. Struct. Mol. Biol.* **15**, 795 (2008). doi:10.1038/nsmb.1468 Medline

17. H. Kim *et al*., Gene-specific RNA polymerase II phosphorylation and the CTD code. *Nat. Struct. Mol. Biol.* **17**, 1279 (2010). doi:10.1038/nsmb.1913 Medline

18. T. J. Creamer *et al*., Transcriptome-wide binding sites for components of the *Saccharomyces cerevisiae* non-poly(A) termination pathway: Nrd1, Nab3, and Sen1. *PLoS Genet.* **7**, e1002329 (2011). doi:10.1371/journal.pgen.1002329 Medline

19. K.-Y. Kim, D. E. Levin, Mpk1 MAPK association with the Paf1 complex blocks Sen1-mediated premature transcription termination. *Cell* **144**, 745 (2011). doi:10.1016/j.cell.2011.01.034 Medline

20. E. J. Steinmetz, N. K. Conrad, D. A. Brow, J. L. Corden, RNA-binding protein Nrd1 directs poly(A)-independent 3′-end formation of RNA polymerase II transcripts. *Nature* **413**, 327 (2001). doi:10.1038/35095090 Medline

21. A. G. Rondón, H. E. Mischo, J. Kawauchi, N. J. Proudfoot, Fail-safe transcriptional termination for protein-coding genes in *S. cerevisiae*. *Mol. Cell* **36**, 88 (2009). doi:10.1016/j.molcel.2009.07.028 Medline

22. A. Meinhart, P. Cramer, Recognition of RNA polymerase II carboxy-terminal domain by 3′-RNA-processing factors. *Nature* **430**, 223 (2004). doi:10.1038/nature02679 Medline

23. B. M. Lunde *et al*., Cooperative interaction of transcription termination factors with the RNA polymerase II C-terminal domain. *Nat. Struct. Mol. Biol.* **17**, 1195 (2010). doi:10.1038/nsmb.1893 Medline

24. M. Sun, L. Larivière, S. Dengl, A. Mayer, P. Cramer, A tandem SH2 domain in transcription elongation factor Spt6 binds the phosphorylated RNA polymerase II C-terminal repeat domain (CTD). *J. Biol. Chem.* **285**, 41597 (2010). doi:10.1074/jbc.M110.144568 Medline

25. M.-L. Diebold *et al*., Noncanonical tandem SH2 enables interaction of elongation factor Spt6 with RNA polymerase II. *J. Biol. Chem.* **285**, 38389 (2010). doi:10.1074/jbc.M110.146696 Medline

26. D. Close *et al*., Crystal structures of the *S. cerevisiae* Spt6 core and C-terminal tandem SH2 domain. *J. Mol. Biol.* **408**, 697 (2011). doi:10.1016/j.jmb.2011.03.002 Medline

27. J. Liu *et al*., Solution structure of tandem SH2 domains from Spt6 protein and their binding to the phosphorylated RNA polymerase II C-terminal domain. *J. Biol. Chem.* **286**, 29218 (2011). doi:10.1074/jbc.M111.252130 Medline

28. S. Buratowski, The CTD code. *Nat. Struct. Mol. Biol.* **10**, 679 (2003). doi:10.1038/nsb0903-679

29. S. Egloff, S. Murphy, Cracking the RNA polymerase II CTD code. *Trends Genet.* **24**, 280 (2008). doi:10.1016/j.tig.2008.03.008 Medline

30. M. L. West, J. L. Corden, Construction and analysis of yeast RNA polymerase II CTD deletion and substitution mutations. *Genetics* **140**, 1223 (1995). Medline

31. C. Blattner *et al*., Molecular basis of Rrn3-regulated RNA polymerase I initiation and cell growth. *Genes Dev.* **25**, 2093 (2011). doi:10.1101/gad.17363311 Medline

32. Z. A. Knight, K. M. Shokat, Features of selective kinase inhibitors. *Chem. Biol.* **12**, 621 (2005). doi:10.1016/j.chembiol.2005.04.011 Medline

33. L. David *et al*., A high-resolution map of transcription in the yeast genome. *Proc. Natl. Acad. Sci. U.S.A.* **103**, 5320 (2006). doi:10.1073/pnas.0601091103 Medline

34. U. Nagalakshmi *et al*., The transcriptional landscape of the yeast genome defined by RNA sequencing. *Science* **320**, 1344 (2008); 10.1126/science.1158441. doi:10.1126/science.1158441 Medline

35. H. Qiu, C. Hu, A. G. Hinnebusch, Phosphorylation of the Pol II CTD by KIN28 enhances BUR1/BUR2 recruitment and Ser2 CTD phosphorylation near promoters. *Mol. Cell* **33**, 752 (2009). doi:10.1016/j.molcel.2009.02.018 Medline